ECOLOGY

Extreme precipitation reshapes nutrient flows and balance in North America's largest river basin

Zihao Bian[1,2], Shufen Pan[2,3], Ge Sun[4], Steven G. McNulty[4], Xingchen Tony Wang[5], Changchun Huang[1], Hanqin Tian[2,5]*

Extreme precipitation events, intensified by climate change, are increasingly disrupting nutrient dynamics in large river systems worldwide. Beyond altering the magnitude of individual nutrient fluxes, extreme precipitation may fundamentally reshape nutrient composition and stoichiometric balances, with critical implications for aquatic ecosystem health. Here, we apply an integrated data-model framework to assess how these events have altered nitrogen (N) and phosphorus (P) fluxes across the Mississippi River Basin from 1980 to 2018. We find that extreme rainfall disproportionately increases P export relative to N, driven primarily by enhanced soil erosion and mobilization of particulate-bound nutrients. Concurrent temporal and spatial changes in extreme precipitation regimes have induced declining N:P ratios in headwater streams and cumulative nutrient loads, shifting export stoichiometry toward the Redfield ratio. Therefore, extreme precipitation can increase nutrient fluxes that fuel harmful algal blooms, yet at the same time reduce N:P ratios that may favor less toxic communities. This trade-off calls for watershed management strategies that go beyond managing nutrient quantity alone.

INTRODUCTION

Human activities have disturbed nutrient cycles and induced nitrogen: phosphorus (N:P) imbalances across the globe (*1*, *2*). The increases in the average N:P ratio of anthropogenic inputs into the biosphere have changed community compositions, diversity, and functions in natural ecosystems and threatened food security and public health in human societies (*3*). Increased land-derived nutrient loading has contributed to the eutrophication and hypoxia in freshwater and marine ecosystems worldwide (*4*). In addition, the disturbed stoichiometry of nutrient loading can alter algal biodiversity, and a more abundant dinoflagellate harmful algal blooms (HABs) has been detected in coastal waters where N:P ratio is higher than Redfield proportions (*5*). Hypoxia zones in the Gulf of Mexico (or Gulf of America), commonly referred to as "dead zone," are primarily associated with excessive N input from the Mississippi River Basin (MRB), but enriched P also played a role. Controlling both N and P loading from the MRB is recognized as the most prospective strategy in mitigating the dead zone, considering it can also minimize harmful ecological impacts caused by disturbed stoichiometric nutrient balance (*6*). Effective management of stoichiometric nutrient balance in the Gulf of Mexico requires a comprehensive understanding of how environmental factors influence the relative rates of N and P transport.

Although anthropogenic disturbance is recognized as the primary driver of large-spatial N:P ratio variability, it is critical to underscore the impact of climate and hydrological drivers in shaping this variability (*7*). Climate dominates the seasonal and annual variability of riverine nutrient loading by controlling watershed hydrology and influencing nutrient leaching and soil erosion from land (*8*, *9*). As N primarily occurs as soluble forms while P mainly occurs in particulate forms in agricultural soils, N and P loading can show different sensitivity to precipitation and runoff change, causing their stoichiometric ratio to vary with hydrology over multiple time scales (*10*, *11*). Leong *et al.* (*12*) indicated that N:P loading increases with discharge according to the observed monthly nutrient flux data at the Mississippi River mouth. However, the analysis of monthly data may mask the response of N:P loading ratio to short-term variability in precipitation, especially extreme precipitation. More intense and frequent extreme precipitation events have been observed in the U.S. during recent decades, which could be attributed to elevated atmospheric water vapor levels, a consequence of global warming (*13*, *14*). The role of extreme precipitation in contributing carbon and nutrient exports to the Gulf of Mexico has attracted considerable attention. Extreme precipitation events have enhanced the leaching of inorganic N (*15*) and intensified erosional N and P fluxes (*16*). Nevertheless, these studies have mainly focused on assessing the impacts of extreme precipitation on individual elements or particular nutrient species. The responses of different nutrient species and their stoichiometric ratios to extreme precipitation across the entire MRB have not been comprehensively quantified. As the Intergovernmental Panel on Climate Change (IPCC) reports an increasing frequency of extreme precipitation events globally (*17*), understanding how such events influence N:P loading ratios is crucial for improving water quality management worldwide.

Quantifying the N:P loading change under extreme precipitation relies on nutrient flux data at fine time scales (e.g., daily step). However, continuous daily nutrient observations are limited in the MRB, and models are often needed to estimate nutrient loading. The complex and nonlinear changes in nutrient loading driven by extreme precipitation could not be captured by empirical models (*18*). In contrast, process-based land surface models have the advantage of representing the long-term impacts of extreme precipitation on nutrient loading at large spatial scales. To our knowledge, we present the first long-term, basin-wide, daily-resolution quantification of the disproportionate responses of N and P loading to extreme precipitation, using the process-based Dynamic Land Ecosystem Model (DLEM)

[1]State Key Laboratory of Climate System Prediction and Risk Management, Nanjing Normal University, Nanjing 210023, China. [2]Center for Earth System Science and Global Sustainability, Schiller Institute for Integrated Science and Society, Boston College, Chestnut Hill, MA 02467, USA. [3]Department of Engineering, Environmental Studies Program, Boston College, Chestnut Hill, MA 02467, USA. [4]Eastern Forest Environmental Threat Assessment Center, Southern Research Station, U.S. Department of Agriculture Forest Service, Durham, NC 27713, USA. [5]Department of Earth and Environmental Sciences, Boston College, Chestnut Hill, MA 02467, USA.
*Corresponding author. Email: hanqin.tian@bc.edu

integrated with multisource climate and nutrient input datasets (table S1). The model is capable of simulating daily time-step changes in different nutrient species (i.e., inorganic and organic, dissolved and particulate forms) under different precipitation intensities at large spatial scales. We estimated land N and P loading to aquatic ecosystems across the MRB from 1980 to 2018 and compared the N:P loading ratio under extreme precipitation and nonextreme precipitation. Here, extreme precipitation is defined as daily precipitation that exceeds the 95th percentile of all daily precipitation during 1980 to 2018 in each grid (*16*). The goals of this study are to (i) estimate the contributions of extreme precipitation to N and P loading across this period, (ii) identify the spatial hotspots of increase in N and P yields induced by extreme precipitation, and (iii) investigate how and why nutrient composition and stoichiometric ratios change under extreme precipitation. By identifying spatial hotspots and revealing how extreme events alter N:P ratios, our analysis moves beyond traditional load assessments to demonstrate how climatic extremes can reorganize nutrient dynamics and complicate management efforts aimed at reducing HABs in the Gulf of Mexico.

RESULTS AND DISCUSSION

The increased contributions of extreme precipitation to N and P yields

The annual volume of extreme precipitation has intensified since the 1990s in the MRB due to the increased frequency and intensity of extreme precipitation events (Fig. 1, A and B). On average, the frequency of extreme precipitation days within a year has doubled, and daily precipitation on EP days has increased from 30 to 35 mm from 1980 to 2018. Meanwhile, the long-term change in annual total precipitation was not significant ($P = 0.08$). The average percentage of extreme precipitation in annual total increased from 25% in the 1990s to 36% in the 2010s (2010–2018). Extreme precipitation has significantly increased across the majority of the entire basin, with the most pronounced

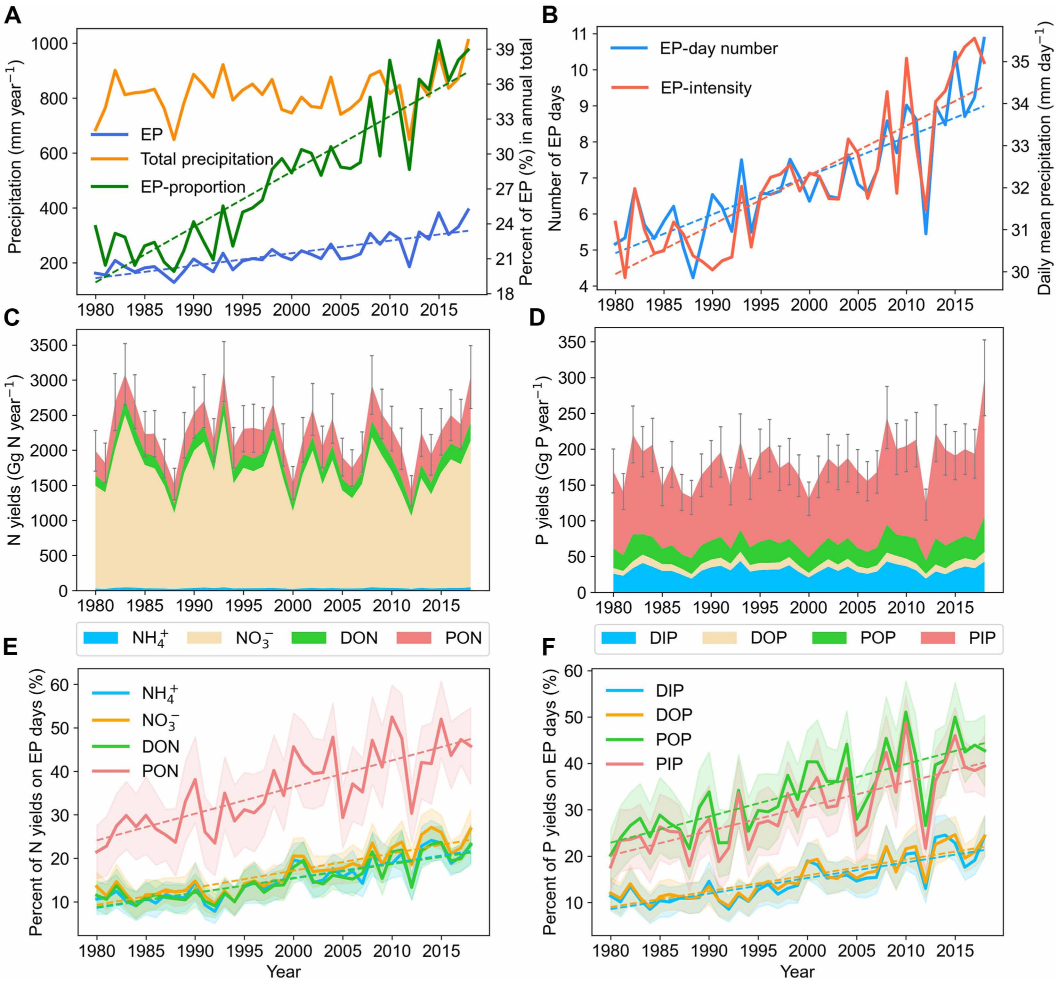

Fig. 1. Temporal dynamics of extreme precipitation and nutrient yields in the MRB during 1980–2018. (**A**) Variations of annual extreme precipitation (EP), total precipitation, and the percentage of extreme precipitation in annual total. (**B**) Interannual variations of the number of days with extreme precipitation (EP days) and daily average extreme precipitation. The interannual changes in total (**C**) N and (**D**) P yields, and the percentages of (**E**) N and (**F**) P yields occurred on EP days in annual total. NH_4^+, ammonium; NO_3^-, nitrate; DON, dissolved organic nitrogen; and PON, particulate organic nitrogen; DIP, dissolved inorganic phosphorus; DOP, dissolved organic phosphorus; POP, particulate organic phosphorus; PIP, particulate inorganic phosphorus. Dash lines in [(A), (B), (E), and (F)] are regression trend lines ($P < 0.05$). Error bars in [(C) and (D)] and shaded bands in [(E) and (F)] around lines represent the uncertainty ranges.

increases observed in the eastern and central regions where forest and cropland are dominant land covers (Fig. 2A and fig. S1).

From 1980 to 2018, both simulated total nitrogen (TN) and total phosphorus (TP) yields fluctuated with precipitation change. While TP yield showed a modest but significant increase from 170 ± 42 Gg P year^{-1} in the 1980s to 205 ± 57 Gg P year^{-1} in the 2010s ($P < 0.05$), TN yield remained relatively stable, averaging 3043 ± 488 Gg N year^{-1} with no significant temporal trend (Fig. 1, C and D). TN yield is mainly composed of dissolved form N, while TP yield is mainly composed of particulate form P. The nitrate (NO_3^-) was the major component of TN yield, but its share has decreased from 76 ± 3% in the 1980s to 71 ± 2% in the 2010s ($P < 0.05$). Meanwhile, the share of particulate organic nitrogen (PON) in TN has increased from 15 ± 3% to 18 ± 3% ($P < 0.05$). Similarly, the share of dissolved inorganic phosphorus (DIP) and particulate inorganic phosphorus (PIP) in TP changed from 17 ± 2% and 62 ± 2% to 15 ± 2% and 64 ± 2%, respectively, from the 1980s to the 2010s. The increase in crop nutrient use efficiency and the decline in nutrient surplus were the major reasons for the decrease in inorganic nutrient loading (*19*). Simultaneously, soil erosion and sediment yield were estimated to increase significantly ($P < 0.05$) within the basin driven by intensified extreme precipitation (fig. S2), resulting in the enhanced yields of particulate form nutrients.

The simulated N and P loading to aquatic ecosystems (i.e., N and P yields in the MRB) that occurred during days with extreme precipitation (EP days) were identified as extreme precipitation–induced nutrient loading. Stimulated by intensified extreme precipitation, N and P yields that occurred on EP days have also increased since the 1990s (fig. S3). The contribution of extreme precipitation to annual N and P yields almost doubled from 1980 to 2018 (Fig. 1, E and F). Extreme precipitation facilitated more particulate form nutrient yields than dissolved form nutrient yields. The percentage of PON, particulate organic phosphorus (POP), and PIP yields occurred on extreme precipitation days in annual totals reached around 42 ± 12% in the 2010s, which is two times that of other dissolved form nutrients. In addition, the proportions of EP-induced particulate form nutrients in total nutrients increased (at a speed of 0.5 to 0.6% year^{-1}) faster than that of EP-induced dissolved form nutrients (around 0.3 to 0.4% year^{-1}) during 1980 to 2018. The major pathway of particulate form nutrients entering aquatic ecosystems is through sedimentation and soil erosion, which is sensitive to extreme precipitation (*20*–*22*). The increased EP events disproportionally favored nutrient loss through erosion process than through leaching process. Overall, the contribution of extreme precipitation to TN yield was estimated to grow from 14 ± 5% in the 1980s to 28 ± 7% in the 2010s, and its contribution to TP yield increased from 21 ± 7% to 36 ± 9%. Because of the large proportion of particulate form P in TP, extreme precipitation preferentially intensified P yield over N across the land-aquatic interface.

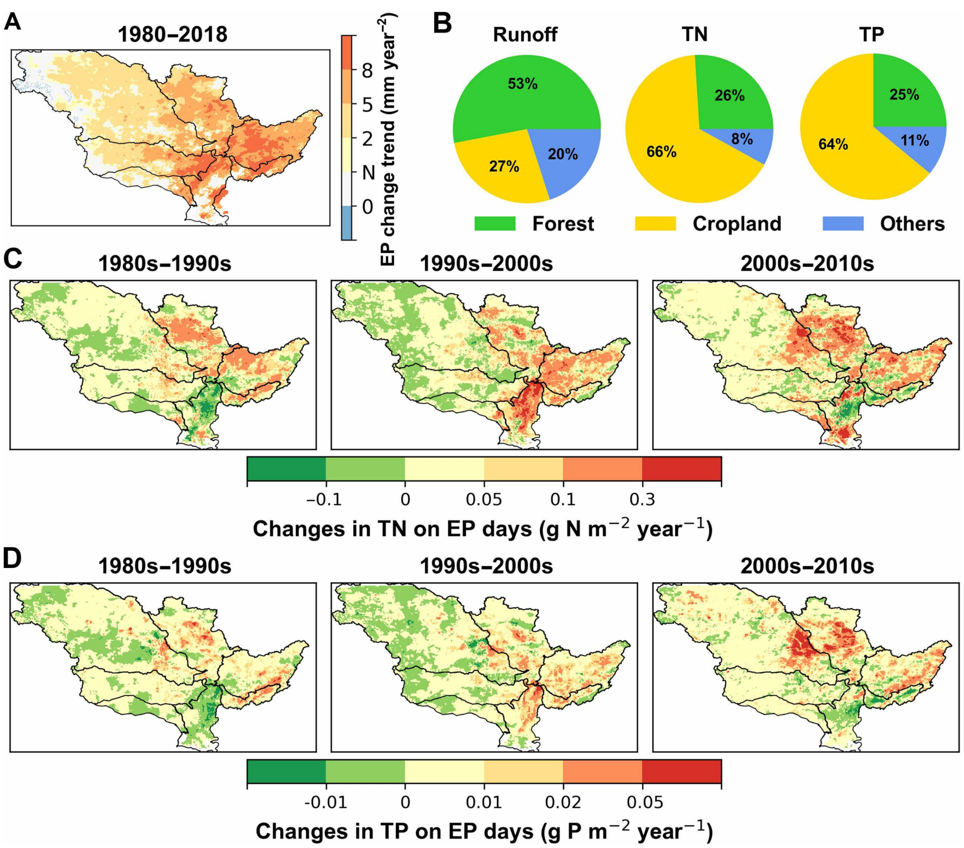

Fig. 2. Changes in spatial patterns of extreme precipitation and associated nutrient yields across the MRB. (**A**) Change trend in extreme precipitation (EP) during 1980 to 2018. The trends were calculated by using linear regressions and verified by the Mann-Kendall test with a significant value of 0.05. N in the color bar refers to no significant trend in EP change. (**B**) Contributions of forest, cropland, and other land use types to water and nutrient yields on EP days in the MRB. (**C** and **D**) The spatial changes in decadal average TN and TP yields occurred on EP days from the 1980s to the 1990s, from the 1990s to the 2000s, and from the 2000s to the 2010s.

Spatial pattern shifts in extreme precipitation events and nutrient yields

The spatial patterns of TN and TP yields induced by extreme precipitation are jointly determined by the distributions of extreme precipitation and land use conditions. The high magnitudes and widespread increases of simulated TN and TP yields induced by EP occurred in the Lower Mississippi, Upper Mississippi, eastern Missouri, and Ohio subbasins (fig. S4). Notably, these subbasins exhibited high nutrient yields originating from cropland areas, a characteristic attributed to substantial anthropogenic nutrient inputs and soil's susceptibility to erosion. Averaged over 1980 to 2018, cropland contributed only 27% of water to total water yield occurred on EP days yet contributed 66% of TN and 64% of TP to total nutrient yields occurred on EP days (Fig. 2B). In contrast, 53% of water yield, 26% of TN yield, and 25% of TP yields during EP events were generated on forests. Nutrient yields, especially dissolved inorganic form and particulate form N and P, are less sensitive to extreme precipitation on forests compared to cropland.

The extreme precipitation experienced a spatial pattern shift in the recent three decades, further exacerbating TN and TP yields over the MRB (Fig. 2, C and D). From the 1990s to the 2000s, the increase in extreme precipitation mainly occurred in the Lower Mississippi and Ohio subbasins. These regions are characterized by forest coverage across the majority of their land area, excluding the Mississippi River Valley (fig. S1). Thus, the enhanced extreme precipitation only had limited impacts on total nutrient loading from the entire MRB. However, from the 2000s to the 2010s, a noticeable intensification of extreme precipitation events occurred in the Midwest, the primary agricultural region in the U.S. The overlap of intensified EP and cropland resulted in extensive increases in nutrient yields in the 2010s, with changes exceeding 0.3 g N m^{-2} $year^{-1}$ for TN and 0.05 g P m^{-2} $year^{-1}$ for TP on EP days (Fig. 2, C and D).

Response of N:P yield ratio to extreme precipitation events

Extreme precipitation can enhance both the leaching of dissolved form N and P (DN and DP) as well as the erosion of particulate form N and P (PN and PP), yet exerts distinct influences on the N:P ratio across total, dissolved, and particulate nutrient yields. The TN:TP ratio of nutrient yields on EP days (20 ± 2) was significantly lower than that on non-EP days (31 ± 4), particularly on cropland (Fig. 3B). In contrast, the average DN:DP and PN:PP ratios of nutrient yields on EP days were slightly higher than those on non-EP days, mainly due to the EP-induced high DN:DP and PN:PP ratios of nutrient yields on forests (Fig. 3, C and D). On the other hand, EP disproportionately favored particulate form nutrients over dissolved form nutrients. On EP days, PN and PP accounted for 29 ± 3% and 88 ± 1% of TN and TP, respectively, significantly higher than their proportions on non-EP days (13 ± 2% and 73 ± 4%) (Fig. 3, E and F). Average PN:PP ratios ranged from 5 to 10, which was much lower compared with DN:DP ratios (around 50 to 130) (Fig. 3, C and D). Thus, if the proportion of particulate nutrient components increases within the total nutrient loading, the TN:TP ratio may decrease. In general, increases in the DN:DP and PN:PP yield ratios due to extreme precipitation were not as substantial as increases in the share of particulate form nutrients in total nutrients, resulting in the overall decrease in TN:TP ratios of nutrient yields (Fig. 4).

The changes in N:P yield ratio in response to precipitation events are primarily determined by the divergent retention characteristics of inorganic N and P in soil. Inorganic N species (NH_4^+ and NO_3^-) display pronounced solubility and mobility within both soil matrices, whereas inorganic P demonstrates an inclination to adsorb onto soil particles or combine with Fe, Al, Mg, and Ca (*23*). The high mobility of inorganic N compared with inorganic P may make DIN more sensitive to precipitation and runoff changes than DIP. Therefore, DN:DP yield ratio induced by extreme precipitation was higher than that induced by non-EP. The change in PN:PP yield ratio during EP events varied with cropland and forests. In croplands, where N and P inputs are typically nonlimiting, the PN:PP ratio of nutrient yields remains relatively stable and exhibits limited sensitivity to intensified precipitation (*16*, *24*). The relatively high PN:PP ratio of nutrient yields on forests during EP events may be related to the limited supply of P in forest soil. Different from N, which can enter forest ecosystems via biological N fixation, external P inputs into forest ecosystems are notably minimal. EP events can cause a lower TN:TP ratio by enhancing soil erosion and discharging higher concentrations of particulate nutrients compared with non-EP (*25*). The TN:TP ratios within stream waters have been observed to decline with increasing discharge over storm scales in many small watersheds (*7*). This study expands upon this knowledge by demonstrating the impact of EP on N:P loading ratio at a large spatial scale. Furthermore, it is noteworthy that the relationship between TN:TP loading ratio and discharge during EP events may exhibit distinctions compared to those observed over monthly or annual temporal scales. Monthly TN:TP was reported to increase with discharge in intensively fertilized subbasins but showed a negative or less significant relationship with discharge in less fertilized subbasins of the MRB (*12*). The trade-off between the increase in DN:DP and the increase in the proportion of particulate form nutrients may explain the divergent responses observed in different regions. Average high flow plays a more prominent role in promoting DN:DP in heavily fertilized regions, whereas it predominantly contributes to the proportion of particulate form nutrients in less-fertilized areas. Nevertheless, as precipitation intensity reaches a certain threshold, the response of the proportion of particulate nutrient forms to elevated discharge consistently exhibits greater sensitivity compared to the response of DN:DP ratios.

Implications

In contrast to the global trend of increasing N:P ratio, the TN:TP ratio of nutrient loading to the Gulf has shifted from increase to decrease in the latter 1980s (*26*, *27*). Over the last three decades, the annual N:P loading mole ratio has decreased from a high of 28 to a low of 20 which is closer to Redfield ratio (N:P = 16), as a consequence of the decrease in TN loading and increase in TP loading. The N:P ratio of synthetic fertilizer inputs rose rapidly during the 1980s and then increased more gradually until reaching a stable level after 2000 in the MRB (fig. S5). Therefore, anthropogenic nutrient input changes alone cannot explain the observed decline in N:P loading. As the nutrient use efficiency of crops continues increasing, the nutrient surplus in the MRB started to decrease; however, legacy nutrients from historical nutrient accumulation in terrestrial ecosystems can still serve as a long-term nutrient source for the coastal regions (*28*). Bian *et al.* (*29*) suggested that the longer residence time of legacy P in soil than N may be the major reason for the decline in N:P loading ratio to the Gulf. This study indicated that the temporal and spatial variations in EP can alter the relative transport of soil residue N versus P and further stimulate the decreasing N:P loading ratio. Because of the strong adsorption of P in soil, sedimentation is the primary pathway of legacy P loss to aquatic ecosystems. The enhanced soil erosion due to the intensified extreme precipitation can

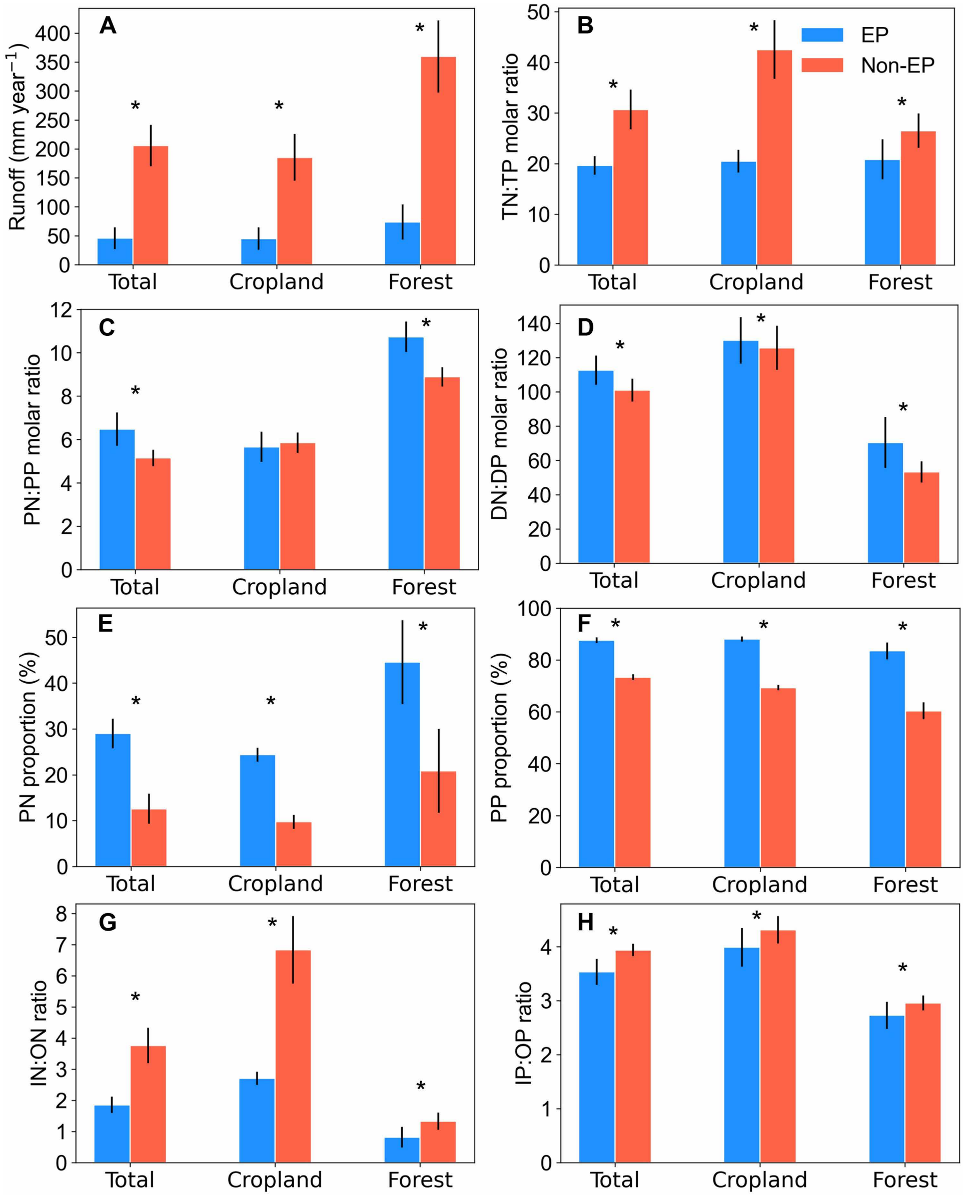

Fig. 3. Comparison of nutrient yield characteristics between EP and non-EP days (1980–2018) on cropland, forest, and the entire MRB. (**A**) Average water yield, (**B**) TN:TP molar ratio, (**C**) particulate nitrogen to particulate phosphorus (PN:PP) molar ratio, (**D**) dissolved nitrogen to dissolved phosphorus (DN:DP) molar ratio, (**E**) proportion of PN in TN yield, (**F**) proportion of PP in TP yield, (**G**) inorganic-to-organic nitrogen (IN:ON) ratio, and (**H**) inorganic-to-organic phosphorus (IP:OP) ratio. The error bar represents the standard deviations of annual data during 1980 to 2018. Asterisks indicate statistically significant differences between extreme and nonextreme precipitation groups at each land type based on a *t* test ($P < 0.05$).

largely mobilize soil legacy source P and contribute to P loading. The increasing TP export to the Gulf of Mexico after the 1990s largely resulted from the enhanced PP loading due to the increased extreme precipitation. It can also explain the continuous increase in TP loss from land to U.S. rivers over the past four decades (*30*). In contrast, the increased PN cannot offset the decrease of DIN because of the small share of PN in TN (Fig. 1C). Therefore, the increases in the frequency and intensity of extreme precipitation since the 1990s have facilitated soil P loss over N, which could contribute to the decline in N:P loading ratio to the Gulf. This mechanism identified in the MRB is likely operating globally, and nutrient stoichiometry shifts driven by climate extremes can have broad implications for lakes, estuaries, and coastal waters worldwide.

Climate change, particularly extreme precipitation, influences both the quantity and proportion of nutrients, potentially altering HABs in complex ways. On the one hand, by mobilizing and transporting large pulses of N and P, extreme precipitation substantially increases nutrient availability, thereby fueling bloom development (*31*). On the other hand, EP-driven runoff induced the lower N:P loading ratio, which can shift algal community composition and, in some cases, reduce the prevalence of highly toxic taxa (*5*). Shifts in elemental ratios can alter algal community structure by changing the competitive balance among

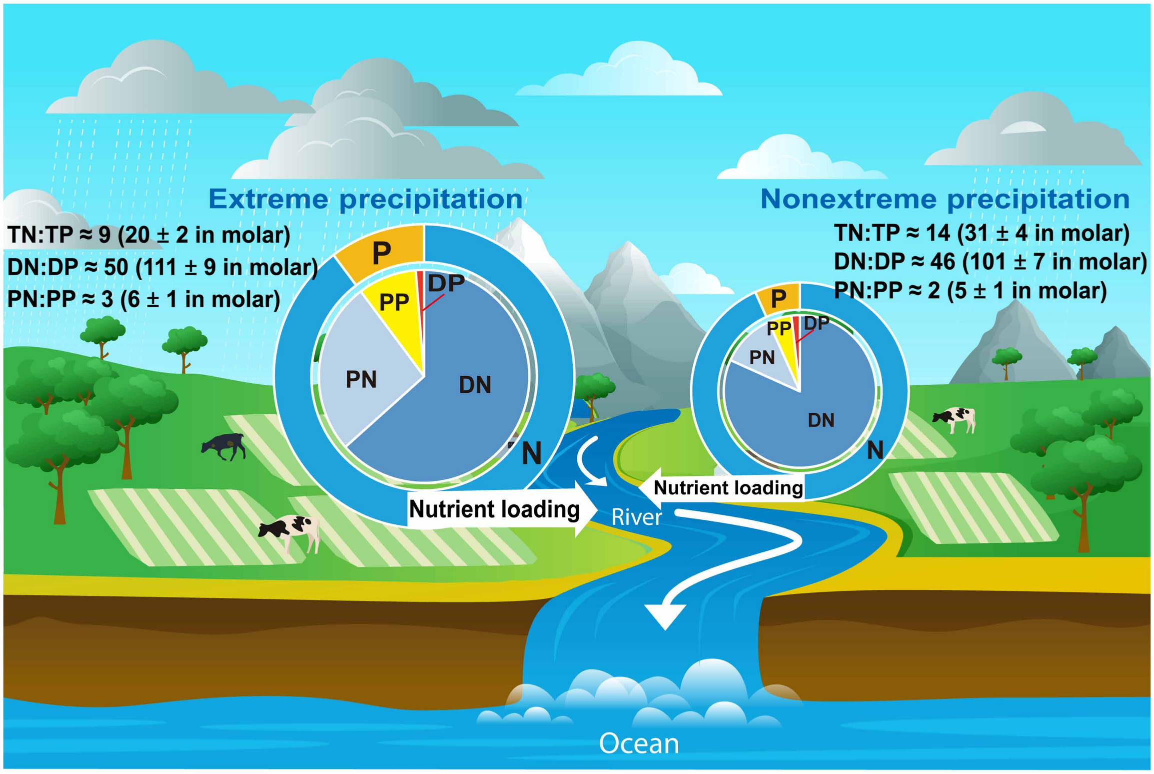

Fig. 4. Differences in proportions of divergent nutrient species and N:P ratio in nutrient loading under extreme and nonextreme precipitation regimes. The sector in the pie chart represents the mass percentage of each nutrient species, and the size of the pie chart indicates the magnitude of nutrient loading.

taxa with differing optimal nutrient requirements. Optimal N:P ratios vary among major groups, with relatively low molar averages for diatoms and dinoflagellates (around 15) and higher values for cyanobacteria and chlorophytes (around 26) (*32*). As N:P loading ratio in the MRB decreased from 28 to 20, the cyanobacteria and chlorophytes could be outcompeted by species with lower optimal N:P ratio. Many regional studies have reported that toxic cyanobacteria and dinoflagellate HABs increase in frequency and abundance under elevated N:P conditions in estuarine and marine waters (*33*, *34*). On the contrary, HABs potentially become less toxic where nutrients change toward balanced (Redfield) proportions. Currently, studies that focus on the impact of extreme precipitation and HABs were mostly conducted in freshwater ecosystems and for short-term periods (*31*, *35*, *36*). The effects of long-term change in N:P ratio induced by extreme precipitation and coastal HABs remain scarce in the literature. It highlights the need for further research to improve the understanding of the relationship between extreme precipitation and coastal HAB dynamics, especially toxin production.

Extreme precipitation also alters the compositional characteristics of nutrients, introducing multiple disturbances to aquatic ecosystems. The flux of particulate-bound nutrients rises sharply during extreme precipitation events, and a substantial fraction of riverine particulates could initially settle near the estuary. The gradual desorption and remineralization of these particles can sustain inorganic nutrient availability in river plumes, serving as a persistent reservoir that fuels algal productivity over extended timescales (*37*). The proportion of terrestrial organic matter in total nutrients also increased during EP days (Fig. 3, G and H). Organic matter is increasingly recognized as a key regulator of aquatic ecosystem productivity through influencing light conditions and carbon availability (*38*). Increased terrestrial organic matter input can drive a shift of aquatic ecosystems from autotrophic to heterotrophic regimes, while simultaneously reshaping the interactions between benthic and pelagic habitats (*39*).

Both total and extreme precipitation are projected to increase across most areas in the Midwest by the end of this century (*40*, *41*), but their impacts vary across different nutrient forms. Historical results indicate that extreme precipitation exerts a stronger influence on N:P ratios than total precipitation (fig. S6). Increases in total precipitation enhance baseline nutrient export, while intensifying extreme precipitation events disproportionately mobilize particulate-bound nutrient and thereby modify stoichiometric nutrient balance. Future precipitation changes are projected to increase TN loading to the Gulf by $1 \pm 8\%$, $6 \pm 8\%$, and $2 \pm 10\%$, and TP loading by $2 \pm 10\%$, $11 \pm 12\%$, and $6 \pm 14\%$ from the 2020s to the 2090s under the SSP1-2.6, SSP3-7.0, and SSP5-8.5 scenarios, respectively (fig. S7). Meanwhile, the intensification of extreme precipitation is projected to result in a $0 \pm 3\%$, $4 \pm 3\%$, and $3 \pm 4\%$ decrease in the TN:TP loading ratio, respectively, under three future scenarios. The projected increases in TN and TP loading, accompanied by a decline in the TN:TP ratio under future climate change, are likely to exacerbate eutrophication risks and alter algal community composition and toxin production in the Gulf. We have to take the future extreme climate into account when making plans and efforts to mitigate nutrient loading and hypoxia in the Gulf.

Residual nutrients on agricultural land are susceptible to extreme precipitation events and subsequent flushing and soil erosion, especially after drought periods (*18*, *42*). Increased extreme precipitation has intensified N and P fluxes to the Gulf of Mexico and poses challenges to the ambitious nutrient reduction goals set by the Hypoxia Task Force (*15*, *43*). Although N is identified as the primary limiting nutrient of the Gulf ecosystem, a dual-nutrient management strategy offers a more efficient pathway, decreasing the N reductions necessary to attain desired ecological outcomes (*44*). However, the increasing frequency and intensity of extreme precipitation disproportionately mobilize particulate P, driving higher P fluxes to the Gulf and underscoring the need to expand management efforts beyond N-focused reduction targets. Aside from coastal ecosystems, eutrophication risks can also increase during EP events in freshwater ecosystems where primary production is mostly limited by P (*45*, *46*). Given that P loading is more sensitive to increased EP events compared to N, high P-load anomalies occurring in EP events have the potential to threaten the ecosystem health of inland water. To meet long-term water-quality goals, management frameworks must explicitly account for the effects of extreme precipitation on the mobilization of residual soil nutrients.

Spatially explicit analysis revealed that the Ohio (27%), Lower Mississippi (24%), and Upper Mississippi (23%) subbasins are the primary contributors to TN loading, whereas the Missouri (36%), Ohio (25%), and Upper Mississippi (19%) subbasins dominate TP loading (Fig. 2 and fig. S8). Most areas within these subbasins also show a significant decline in the TN:TP loading ratio. These hotspot patterns persist under extreme precipitation conditions, highlighting their importance as priority regions for nutrient management. Optimal utilization of best management practices within these basins, including cover management, riparian buffer strips, and reduced tillage, are necessary to prevent soil erosion and associated legacy nutrient mobilization under the future extreme climate. In addition, considering the benefits offered by forests in terms of soil erosion control and water quality improvement (*47*), the preservation of currently forested areas or the restoration of forests through reforestation will gain importance in regions where an increase in extreme precipitation is anticipated in the coming years. Moreover, future monitoring networks may need to adapt to capture storm-driven fluxes more effectively, moving beyond monthly sampling toward event-based or high-frequency monitoring. Modeling frameworks can also be enhanced by improved representation of hydrologic modifications (e.g., tile drainage and dams) and management interventions under projected increases in extreme precipitation. Collectively, these efforts can better support watershed management strategies that move beyond annual load targets to explicitly address the nutrient export dynamics driven by extreme precipitation events and their associated ecological consequences.

MATERIALS AND METHODS

In this study, the DLEM was integrated with multiple collected datasets of N inputs, P inputs, land use, and climate to create a comprehensive data-model framework for simulating nutrient dynamics in response to extreme climate. The observed riverine nutrient flux data were used to calibrate and validate this framework. Detailed information on the model and input data is provided as follows:

Dynamic Land Ecosystem Model

The DLEM is a process-based model coupling water, C, N, and P cycles across terrestrial and aquatic systems (*29*, *48*, *49*) (fig. S9). Within the land component of the DLEM, the C, N, and P are coupled during photosynthesis, allocation, turnover, nutrient uptake, and decomposition processes in terrestrial ecosystems. Other key N-related processes in the land component include nitrification, denitrification, volatilization, and N fixation (*50*). Meanwhile, P-related processes include weathering, adsorption, desorption, and occlusion (*51*). Key hydrological processes in the land component include canopy interception, canopy evapotranspiration, soil evaporation, infiltration, and soil moisture dynamics, as well as surface runoff and drainage generation. The DLEM is a grid cell–based and fully distributed model. In this study, simulations were conducted at a spatial resolution of 5 × 5 arc min with a daily time step. To capture subgrid-scale processes, a cohort-based structure was implemented, partitioning each grid cell into seven land cover types: vegetation, impervious surfaces, bare ground, glaciers, lakes, streams, and seas. The vegetation cover comprises up to five plant functional types, with one designated for crops and the remaining four for natural vegetation.

Nutrient cycles in land and aquatic components are connected through leaching, soil erosion, and wastewater discharge (detailed equations can be found in text S1). External nutrient inputs to this land-aquatic system include synthetic fertilizer, livestock manure, atmospheric deposition, and biological nitrogen fixation (BNF). Nitrogen loading to aquatic ecosystems mainly consists of four N species: ammonium (NH_4^+), NO_3^-, dissolved organic nitrogen (DON), and PON, while P loading also consists of four species: DIP, dissolved organic phosphorus (DOP), PIP, and POP. The leaching and soil erosion contributed to dissolved form and particulate form nutrient loading, respectively. The organic form and inorganic form of N and P in aquatic ecosystems are derived from soil organic nutrient pools and inorganic nutrient pools, respectively. The nutrient yields reported in this study specifically represent the transfer of nutrients from the terrestrial system to the aquatic system.

Within the aquatic component, nutrients are transported through hillslope flow, subnetwork flow, and main-channel flow until river outlets based on a scale-adaptive water transport scheme (Model of Scale Adaptive River Transport) (*52*, *53*). Simultaneously, the biogeochemical cycling of N and P within stream networks was quantified, encompassing processes such as mineralization of organic N and P, deposition of particulate form N and P, assimilation of inorganic N and P, nitrification and denitrification of inorganic N, as well as adsorption and desorption dynamics between dissolved and particulate phases (text S1). These processes were systematically assessed across inland water systems within each grid cell.

Legacy nutrient processes are explicitly represented in the DLEM framework mainly through the long-term nutrient accumulation within the terrestrial-aquatic ecosystems. Nutrient accumulation is determined by the balance between nutrient inputs (synthetic fertilizer, livestock manure, atmospheric deposition, weathering P, and BNF) and outputs (crop harvest, N gas emissions, and nutrient loading) during the historical simulation over 1901 to 2018 (fig. S10). Our estimated nutrient inputs and outputs in the MRB are comparable with previous studies (*26*, *54*, *55*). Legacy nutrients are mainly tracked in soil inorganic and organic pools with distinct turnover times (fig. S9). Extreme precipitation can induce the mobilization of legacy nutrients through leaching and soil erosion processes (text S1). The capacity of DLEM in capturing the impact of soil legacy nutrients on nutrient loading has been reported in our recent study (*29*).

Environmental forcing data

Natural and human forcings driving the DLEM include climate, soil properties, topography, river network, land use change, atmospheric CO_2, synthetic fertilizer nutrient input, livestock manure nutrient input, atmospheric nutrient deposition, and wastewater discharge (table S1). The daily climate inputs, including precipitation and temperature, etc., were acquired from GRIDMET. We used the grid-level annual fertilizer and manure nutrient input datasets developed by Cao *et al.* (*56*) and Bian *et al.* (*57*). The fertilizer nutrient data were developed by downscaling state-level crop-specific nutrient application rates of nine crops (wheat, corn, rice, soybean, cotton, sorghum, barley, oats, and peanut) based on crop density and rotation maps. Similarly, manure nutrient production and application data were developed by combining county-level livestock numbers, livestock nutrient excretion rates, livestock distribution maps, and crop density maps. We used high-resolution annual crop density maps (*58*), annual urban area maps, and a potential vegetation map to generate the land use forcing. The land use change were assumed to be dominated by cropland expansion and abandonment and urbanization. All these forcing datasets were developed or resampled to a spatial resolution of 5 × 5 arc min.

Model evaluation

The DLEM has been successfully applied to simulate long-term water, sediment, N, and P dynamics along the land-ocean continuum in the MRB in response to climate and anthropogenic activities (*29*, *59*–*61*). The DLEM has demonstrated good performance in simulating N and P exports from the MRB to the Gulf of Mexico, as evaluated against the WRTDS-computed nutrient loads provided by U.S. Geological Survey (USGS) (fig. S11). The model captures long-term trends and variations of annual riverine N and P fluxes effectively. In our previous studies, we have already calibrated the DLEM and verified the capabilities in simulating discharge, riverine N fluxes (*59*), riverine P fluxes (*60*), and sediment yield (fig. S12) (*62*) in the MRB by comparing simulated monthly fluxes with USGS observations across the major subbasins in the MRB. The Nash-Sutcliffe efficiency (NSE) values for the DLEM model's performance in simulating nutrient exports varied across different nutrient forms and subbasins (tables S2 and S3). In general, DLEM showed relatively good agreement with observations for NO_3^- (NSE: 0.17 to 0.69) in most subbasins but weaker performance in simulating NH_4^+ (NSE: −0.42 to 0.3) due to high variability in observational data. NSE values of total organic nitrogen simulation ranged from 0.06 to 0.69, with reasonable agreement but some inconsistencies at certain sites. For riverine P fluxes, DLEM simulations of DIP (NSE: 0.32 to 0.59) and TP (NSE: 0.21 to 0.65) exports were generally consistent with USGS observations. However, TP export was slightly overestimated in certain regions, such as the Arkansas River, while DIP fluxes showed minor underestimation in the Upper Mississippi River. Overall, model performance varied among nutrient forms. Simulations of NH_4^+ and DIP exhibited larger bias due to differences in data availability and model process representation. Nevertheless, because TP and NO_3^- (the dominant component in TN export) are more reliably represented, the overarching conclusions regarding total nutrient fluxes and shifts in N:P stoichiometry under extreme precipitation remain robust. Future improvements should focus on refining NH_4^+ transport mechanisms and improving the representation of hydrologic modifications (e.g., tile drainage and dams) to enhance model performance. In addition, model development will aim to incorporate management practices, thereby enhancing its utility for guiding adaptive nutrient management and policy decisions under a changing climate.

Definition of extreme precipitation

In this study, we defined extreme precipitation as daily precipitation that exceeds the 95th percentile of all daily precipitation (>0.1 mm) during 1980 to 2018 in each grid (*16*). In contrast, precipitation less than the 95th percentile threshold was defined as nonextreme precipitation. The total extreme precipitation at each grid cell is determined by summing the precipitation from all extreme rainfall days within a given year. The simulated N and P loading from land to aquatic ecosystems that occurred during days with extreme precipitation were identified as extreme precipitation–induced nutrient loading. This definition allows spatial comparison across a large spatial scale but potentially underestimates the EP-induced nutrient loading, as heavy rainfall events can lead to a consistently high baseflow and soil nutrient leaching over the following days.

Uncertainty and sensitivity analysis

Uncertainty in simulated nutrient loading arises from multiple sources, including model structure, parameterization, forcing datasets, and the definition of extreme precipitation. Here, we quantified the uncertainty associated with parameterization and the definition of extreme precipitation using a multifactor ensemble approach. To assess sensitivity to the definition of extreme precipitation, we defined extreme precipitation events using the 90th, 95th, and 99th percentiles of daily precipitation (>0.1 mm) for each grid cell during 1980 to 2018, resulting in three extreme precipitation scenarios. For parameter uncertainty, we selected five key parameters in the DLEM (table S4) that strongly influence the yields of different nutrient forms. On the basis of prior calibration and validation at subbasin outlets, each parameter was varied within ±20% of its optimized value to capture empirical uncertainty while maintaining model stability. The model was run for each combination of parameter set and extreme precipitation scenarios, generating a two-dimensional ensemble of simulated N and P loading. The 95% confidence interval for each simulated variable was then estimated from the ensemble distribution using a two-tailed *t* test, representing the total uncertainty range.

Supplementary Materials

This PDF file includes:
Supplementary Text
Figs. S1 to S12
Tables S1 to S4
References

REFERENCES

1. A. F. Bouwman, A. H. W. Beusen, G. Billen, Human alteration of the global nitrogen and phosphorus soil balances for the period 1970–2050. *Global Biogeochem. Cycles* **23**, GB0A04 (2009).
2. J. Peñuelas, J. Sardans, The global nitrogen-phosphorus imbalance. *Science* **375**, 266–267 (2022).
3. J. Peñuelas, B. Poulter, J. Sardans, P. Ciais, M. van der Velde, L. Bopp, O. Boucher, Y. Godderis, P. Hinsinger, J. Llusia, E. Nardin, S. Vicca, M. Obersteiner, I. A. Janssens, Human-induced nitrogen–phosphorus imbalances alter natural and managed ecosystems across the globe. *Nat. Commun.* **4**, 2934 (2013).
4. J. C. Ho, A. M. Michalak, N. Pahlevan, Widespread global increase in intense lake phytoplankton blooms since the 1980s. *Nature* **574**, 667–670 (2019).
5. P. M. Glibert, Eutrophication, harmful algae and biodiversity—Challenging paradigms in a world of complex nutrient changes. *Mar. Pollut. Bull.* **124**, 591–606 (2017).
6. W. K. Dodds, Nutrients and the "dead zone": The link between nutrient ratios and dissolved oxygen in the northern Gulf of Mexico. *Front. Ecol. Environ.* **4**, 211–217 (2006).
7. M. B. Green, J. C. Finlay, Patterns of hydrologic control over stream water total nitrogen to total phosphorus ratios. *Biogeochemistry* **99**, 15–30 (2010).

8. T. C. Ballard, E. Sinha, A. M. Michalak, Long-term changes in precipitation and temperature have already impacted nitrogen loading. *Environ. Sci. Technol.* **53**, 5080–5090 (2019).
9. E. Sinha, A. M. Michalak, Precipitation dominates interannual variability of riverine nitrogen loading across the continental United States. *Environ. Sci. Technol.* **50**, 12874–12884 (2016).
10. J.-O. Goyette, E. M. Bennett, R. Maranger, Differential influence of landscape features and climate on nitrogen and phosphorus transport throughout the watershed. *Biogeochemistry* **142**, 155–174 (2019).
11. M. C. Ockenden, C. E. Deasy, C. McW, H. Benskin, K. J. Beven, S. Burke, A. L. Collins, R. Evans, P. D. Falloon, K. J. Forber, K. M. Hiscock, M. J. Hollaway, R. Kahana, C. J. A. Macleod, S. M. Reaney, M. A. Snell, M. L. Villamizar, C. Wearing, P. J. A. Withers, J. G. Zhou, P. M. Haygarth, Changing climate and nutrient transfers: Evidence from high temporal resolution concentration-flow dynamics in headwater catchments. *Sci. Total Environ.* **548-549**, 325–339 (2016).
12. D. N. S. Leong, S. D. Donner, M. A. Hassan, R. Gabor, J. D. Drummond, Sensitivity of stoichiometric ratios in the Mississippi River to hydrologic variability. *J. Geophys. Res.* **119**, 1049–1062 (2014).
13. E. Janssen, D. J. Wuebbles, K. E. Kunkel, S. C. Olsen, A. Goodman, Observational- and model-based trends and projections of extreme precipitation over the contiguous United States. *Earth's Future.* **2**, 99–113 (2014).
14. K. M. Willett, N. P. Gillett, P. D. Jones, P. W. Thorne, Attribution of observed surface humidity changes to human influence. *Nature* **449**, 710–712 (2007).
15. C. Lu, J. Zhang, H. Tian, W. G. Crumpton, M. J. Helmers, W.-J. Cai, C. S. Hopkinson, S. E. Lohrenz, Increased extreme precipitation challenges nitrogen load management to the Gulf of Mexico. *Commun. Earth Environ.* **1**, 1–10 (2020).
16. Z. Tan, L. R. Leung, H.-Y. Li, T. Tesfa, Q. Zhu, X. Yang, Y. Liu, M. Huang, Increased extreme rains intensify erosional nitrogen and phosphorus fluxes to the northern Gulf of Mexico in recent decades. *Environ. Res. Lett.* **16**, 054080 (2021).
17. H. Lee, K. Calvin, D. Dasgupta, G. Krinner, A. Mukherji, P. Thorne, C. Trisos, J. Romero, P. Aldunce, K. Barret, IPCC, 2023: Climate change 2023: Synthesis report, summary for policymakers. Contribution of working groups i, II and III to the sixth assessment report of the intergovernmental panel on climate change [core writing team, h. Lee and j. Romero (eds.)]. (IPCC, Geneva, Switzerland, 2023).
18. M. Lee, E. Shevliakova, S. Malyshev, P. C. D. Milly, P. R. Jaffé, Climate variability and extremes, interacting with nitrogen storage, amplify eutrophication risk. *Geophys. Res. Lett.* **43**, 7520–7528 (2016).
19. R. D. Sabo, C. M. Clark, J. E. Compton, Considerations when using nutrient inventories to prioritize water quality improvement efforts across the US. *Environ. Res. Commun.* **3**, 045005 (2021).
20. R. Coppus, A. C. Imeson, Extreme events controlling erosion and sediment transport in a semi-arid sub-Andean valley. *Earth Surf. Process. Landf.* **27**, 1365–1375 (2002).
21. W. Wei, L. Chen, B. Fu, Y. Lü, J. Gong, Responses of water erosion to rainfall extremes and vegetation types in a loess semiarid hilly area, NW China. *Hyfrol. Process.* **23**, 1780–1791 (2009).
22. Y. Zhao, W. Cao, C. Hu, Y. Wang, Z. Wang, X. Zhang, B. Zhu, C. Cheng, X. Yin, B. Liu, Analysis of changes in characteristics of flood and sediment yield in typical basins of the Yellow River under extreme rainfall events. *Catena* **177**, 31–40 (2019).
23. R. W. McDowell, B. J. F. Biggs, A. N. Sharpley, L. Nguyen, Connecting phosphorus loss from agricultural landscapes to surface water quality. *Chem. Ecol.* **20**, 1–40 (2004).
24. D. W. P. Manning, A. D. Rosemond, J. P. Benstead, P. M. Bumpers, J. S. Kominoski, Transport of N and P in U.S. streams and rivers differs with land use and between dissolved and particulate forms. *Ecol. Appl.* **30**, e02130 (2020).
25. D. L. Correll, T. E. Jordan, D. E. Weller, Transport of nitrogen and phosphorus from rhode river watersheds during storm events. *Water Resour. Res.* **35**, 2513–2521 (1999).
26. S. Stackpoole, R. Sabo, J. Falcone, L. Sprague, Long-term Mississippi River trends expose shifts in the river load response to watershed nutrient balances between 1975 and 2017. *Water Resour. Res.* **57**, e2021WR030318 (2021).
27. R. E. Turner, N. N. Rabalais, D. Justic, Predicting summer hypoxia in the northern Gulf of Mexico: Riverine N, P, and Si loading. *Mar. Pollut. Bull.* **52**, 139–148 (2006).
28. D. Chen, H. Shen, M. Hu, J. Wang, Y. Zhang, R. A. Dahlgren, "Chapter Five - Legacy Nutrient Dynamics at the Watershed Scale: Principles, Modeling, and Implications" in *Advances in Agronomy*, D. L. Sparks, Ed. (Academic Press, 2018), vol. 149, pp. 237–313; http://www.sciencedirect.com/science/article/pii/S0065211318300051.
29. Z. Bian, H. Tian, S. Pan, H. Shi, C. Lu, C. Anderson, W.-J. Cai, C. S. Hopkinson, D. Justic, L. Kalin, S. Lohrenz, S. McNulty, N. Pan, G. Sun, Z. Wang, Y. Yao, Y. You, Soil legacy nutrients contribute to the decreasing stoichiometric ratio of N and P loading from the Mississippi River Basin. *Glob. Change Biol.* **29**, 7145–7158 (2023).
30. W. Zhi, H. Baniecki, J. Liu, E. Boyer, C. Shen, G. Shenk, X. Liu, L. Li, Increasing phosphorus loss despite widespread concentration decline in US rivers. *Proc. Natl. Acad. Sci. U.S.A.* **121**, e2402028121 (2024).
31. E. S. Reichwaldt, A. Ghadouani, Effects of rainfall patterns on toxic cyanobacterial blooms in a changing climate: Between simplistic scenarios and complex dynamics. *Water Res.* **46**, 1372–1393 (2012).
32. H. Hillebrand, G. Steinert, M. Boersma, A. Malzahn, C. L. Meunier, C. Plum, R. Ptacnik, Goldman revisited: Faster-growing phytoplankton has lower N: P and lower stoichiometric flexibility. *Limnol. Oceanogr.* **58**, 2076–2088 (2013).
33. P. M. Glibert, R. Maranger, D. J. Sobota, L. Bouwman, The Haber Bosch–harmful algal bloom (HB–HAB) link. *Environ. Res. Lett.* **9**, 105001 (2014).
34. J. Li, P. M. Glibert, Y. Gao, Temporal and spatial changes in Chesapeake Bay water quality and relationships to *Prorocentrum minimum*, *Karlodinium veneficum*, and CyanoHAB events, 1991–2008. *Harmful Algae* **42**, 1–14 (2015).
35. S. C. Chapra, B. Boehlert, C. Fant, J. V. J. Bierman, J. Henderson, D. Mills, D. M. L. Mas, L. Rennels, L. Jantarasami, J. Martinich, K. M. Strzepek, H. W. Paerl, Climate change impacts on harmful algal blooms in U.S. freshwaters: A screening-level assessment. *Environ. Sci. Technol.* **15**, 8933–8943 (2017).
36. M. L. Larsen, H. M. Baulch, S. L. Schiff, D. F. Simon, S. Sauvé, J. J. Venkiteswaran, Extreme rainfall drives early onset cyanobacterial bloom. *FACETS* **5**, 899–920 (2020).
37. M. Dagg, R. Benner, S. Lohrenz, D. Lawrence, Transformation of dissolved and particulate materials on continental shelves influenced by large rivers: Plume processes. *Cont. Shelf Res.* **24**, 833–858 (2004).
38. I. F. Creed, A.-K. Bergström, C. G. Trick, N. B. Grimm, D. O. Hessen, J. Karlsson, K. A. Kidd, E. Kritzberg, D. M. McKnight, E. C. Freeman, O. E. Senar, A. Andersson, J. Ask, M. Berggren, M. Cherif, R. Giesler, E. R. Hotchkiss, P. Kortelainen, M. M. Palta, T. Vrede, G. A. Weyhenmeyer, Global change-driven effects on dissolved organic matter composition: Implications for food webs of northern lakes. *Glob. Change Biol.* **24**, 3692–3714 (2018).
39. A. Deininger, H. Frigstad, Reevaluating the role of organic matter sources for coastal eutrophication, oligotrophication, and ecosystem health. *Front. Mar. Sci.* **6**, 210 (2019).
40. F. V. Davenport, N. S. Diffenbaugh, Using machine learning to analyze physical causes of climate change: A case study of U.S. midwest extreme precipitation. *Geophys. Res. Lett.* **48**, e2021GL093787 (2021).
41. J. Zhang, C. Lu, W. Crumpton, C. Jones, H. Tian, G. Villarini, K. Schilling, D. Green, Heavy precipitation impacts on nitrogen loading to the gulf of Mexico in the 21st century: Model projections under future climate scenarios. *Earth's Future* **10**, e2021EF002141 (2022).
42. J. Zhang, C. Lu, H. Feng, D. Hennessy, Y. Guan, M. M. Wright, Extreme climate increased crop nitrogen surplus in the United States. *Agric. For. Meteorol.* **310**, 108632 (2021).
43. H. T. Force, Mississippi river/gulf of Mexico watershed nutrient task force 2015 report to congress. *U.S. Environmental Protection Agency* (Washington, DC, 2015); https://www.epa.gov/sites/default/files/2015-10/documents/htf_report_to_congress_final_-_10.1.15.pdf.
44. K. Fennel, A. Laurent, N and P as ultimate and proximate limiting nutrients in the northern Gulf of Mexico: Implications for hypoxia reduction strategies. *Biogeosciences* **15**, 3121–3131 (2018).
45. D. J. Conley, H. W. Paerl, R. W. Howarth, D. F. Boesch, S. P. Seitzinger, K. E. Havens, C. Lancelot, G. E. Likens, Controlling eutrophication: Nitrogen and phosphorus. *Science* **323**, 1014–1015 (2009).
46. R. W. Howarth, F. Chan, D. P. Swaney, R. M. Marino, M. Hayn, Role of external inputs of nutrients to aquatic ecosystems in determining prevalence of nitrogen vs. phosphorus limitation of net primary productivity. *Biogeochemistry* **154**, 293–306 (2021).
47. P. V. Caldwell, K. L. Martin, J. M. Vose, J. S. Baker, T. W. Warziniack, J. K. Costanza, G. E. Frey, A. Nehra, C. M. Mihiar, Forested watersheds provide the highest water quality among all land cover types, but the benefit of this ecosystem service depends on landscape context. *Sci. Total Environ.* **882**, 163550 (2023).
48. S. Pan, Z. Bian, H. Tian, Y. Yao, R. G. Najjar, M. A. M. Friedrichs, E. E. Hofmann, R. Xu, B. Zhang, Impacts of multiple environmental changes on long-term nitrogen loading from the Chesapeake Bay watershed. *J. Geophys. Res.* **126**, e2020JG005826 (2021).
49. H. Tian, G. Chen, M. Liu, C. Zhang, G. Sun, C. Lu, X. Xu, W. Ren, S. Pan, A. Chappelka, Model estimates of net primary productivity, evapotranspiration, and water use efficiency in the terrestrial ecosystems of the southern United States during 1895–2007. *For. Ecol. Manag.* **259**, 1311–1327 (2010).
50. Q. Yang, H. Tian, M. A. Friedrichs, C. S. Hopkinson, C. Lu, R. G. Najjar, Increased nitrogen export from eastern North America to the Atlantic Ocean due to climatic and anthropogenic changes during 1901–2008. *J. Geophys. Res.* **120**, 1046–1068 (2015).
51. Z. Wang, H. Tian, J. Yang, H. Shi, S. Pan, Y. Yao, K. Banger, Q. Yang, Coupling of phosphorus processes with carbon and nitrogen cycles in the dynamic land ecosystem model: model structure, parameterization, and evaluation in tropical forests. *J. Adv. Model. Earth Syst.* **12**, e2020MS002123 (2020).
52. H. Li, M. S. Wigmosta, H. Wu, M. Huang, Y. Ke, A. M. Coleman, L. R. Leung, A physically based runoff routing model for land surface and earth system models. *J. Hydrometeorol.* **14**, 808–828 (2013).
53. Y. Yao, H. Tian, S. Pan, R. G. Najjar, M. A. M. Friedrichs, Z. Bian, H.-Y. Li, E. E. Hofmann, Riverine carbon cycling over the past century in the mid-atlantic region of the United States. *J. Geophys. Res.* **126**, e2020JG005968 (2021).

54. R. D. Sabo, C. M. Clark, J. Bash, D. Sobota, E. Cooter, J. P. Dobrowolski, B. Z. Houlton, A. Rea, D. Schwede, S. L. Morford, J. E. Compton, Decadal shift in nitrogen inputs and fluxes across the contiguous United States: 2002–2012. *J. Geophys. Res.* **124**, 3104–3124 (2019).
55. R. D. Sabo, C. M. Clark, D. A. Gibbs, G. S. Metson, M. J. Todd, S. D. LeDuc, D. Greiner, M. M. Fry, R. Polinsky, Q. Yang, H. Tian, J. E. Compton, Phosphorus inventory for the conterminous United States (2002–2012). *J. Geophys. Res.* **126**, e2020JG005684 (2021).
56. P. Cao, C. Lu, Z. Yu, Historical nitrogen fertilizer use in agricultural ecosystems of the contiguous United States during 1850–2015: Application rate, timing, and fertilizer types. *Earth Syst. Sci. Data* **10**, 969–984 (2018).
57. Z. Bian, H. Tian, Q. Yang, R. Xu, S. Pan, B. Zhang, Production and application of manure nitrogen and phosphorus in the United States since 1860. *Earth Syst. Sci. Data* **13**, 515–527 (2021).
58. Z. Yu, C. Lu, Historical cropland expansion and abandonment in the continental U.S. during 1850 to 2016. *Glob. Ecol. Biogeogr.* **27**, 322–333 (2018).
59. H. Tian, R. Xu, S. Pan, Y. Yao, Z. Bian, W.-J. Cai, C. S. Hopkinson, D. Justic, S. Lohrenz, C. Lu, W. Ren, J. Yang, Long-term trajectory of nitrogen loading and delivery from Mississippi River Basin to the Gulf of Mexico. *Global Biogeochem. Cycles* **34**, e2019GB006475 (2020).
60. Z. Bian, S. Pan, Z. Wang, Y. Yao, R. Xu, H. Shi, L. Kalin, C. Anderson, D. Justic, S. Lohrenz, H. Tian, A century-long trajectory of phosphorus loading and export from Mississippi River Basin to the Gulf of Mexico: Contributions of multiple environmental changes. *Global Biogeochem. Cycles* **36**, e2022GB007347 (2022).
61. M. Liu, H. Tian, Q. Yang, J. Yang, X. Song, S. E. Lohrenz, W.-J. Cai, Long-term trends in evapotranspiration and runoff over the drainage basins of the Gulf of Mexico during 1901–2008. *Water Resour. Res.* **49**, 1988–2012 (2013).
62. Z. Bian, G. Sun, S. McNulty, S. Pan, H. Tian, Understanding the shift of drivers of soil erosion and sedimentation based on regional process-based modeling in the Mississippi River Basin during the past century. *Water Resour. Res.* **59**, e2023WR035377 (2023).
63. D. B. Schwede, G. G. Lear, A novel hybrid approach for estimating total deposition in the United States. *Atmos. Emviron.* **92**, 207–220 (2014).
64. O. Morgenstern, M. I. Hegglin, E. Rozanov, F. M. O'Connor, N. L. Abraham, H. Akiyoshi, A. T. Archibald, S. Bekki, N. Butchart, M. P. Chipperfield, Review of the global models used within phase 1 of the Chemistry–Climate Model Initiative (CCMI). *Geosci. Model Dev.* **10**, 639–671 (2017).
65. N. Mahowald, T. D. Jickells, A. R. Baker, P. Artaxo, C. R. Benitez-Nelson, G. Bergametti, T. C. Bond, Y. Chen, D. D. Cohen, B. Herut, N. Kubilay, R. Losno, C. Luo, W. Maenhaut, K. A. McGee, G. S. Okin, R. L. Siefert, S. Tsukuda, Global distribution of atmospheric phosphorus sources, concentrations and deposition rates, and anthropogenic impacts: GLOBAL ATMOSPHERIC PHOSPHORUS. *Global Biogeochem. Cycles* **22**, GB4026 (2008).
66. H. Wu, J. S. Kimball, H. Li, M. Huang, L. R. Leung, R. F. Adler, A new global river network database for macroscale hydrologic modeling. *Water Resour. Res.* **48**, W09701 (2012).
67. S. L. Neitsch, J. G. Arnold, J. R. Kiniry, J. R. Williams, "Soil and water assessment tool theoretical documentation version 2009," (Texas Water Resources Institute, 2011).
68. J. R. Williams, The EPIC model. *Computer Models of Watershed Hydrology*, 909–1000 (1995).
69. Y. Li, H. Tian, Y. Yao, H. Shi, Z. Bian, Y. Shi, S. Wang, T. Maavara, R. Lauerwald, S. Pan, Increased nitrous oxide emissions from global lakes and reservoirs since the pre-industrial era. *Nat. Commun.* **15**, 942 (2024).
70. M. L. Messager, B. Lehner, G. Grill, I. Nedeva, O. Schmitt, Estimating the volume and age of water stored in global lakes using a geo-statistical approach. *Nat. Commun.* **7**, 13603 (2016).
71. B. Lehner, C. R. Liermann, C. Revenga, C. Vörösmarty, B. Fekete, P. Crouzet, P. Döll, M. Endejan, K. Frenken, J. Magome, C. Nilsson, J. C. Robertson, R. Rödel, N. Sindorf, D. Wisser, High-resolution mapping of the world's reservoirs and dams for sustainable river-flow management. *Front. Ecol. Environ.* **9**, 494–502 (2011).
72. G. Van Drecht, A. F. Bouwman, J. Harrison, J. M. Knoop, Global nitrogen and phosphate in urban wastewater for the period 1970 to 2050. *Global Biogeochem. Cycles* **23**, GB0A03 (2009).
73. G. H. Allen, T. M. Pavelsky, Global extent of rivers and streams. *Science* **361**, 585–588 (2018).
74. C. Homer, J. Dewitz, L. Yang, S. Jin, P. Danielson, G. Xian, J. Coulston, N. Herold, J. Wickham, K. Megown, Completion of the 2011 National Land Cover Database for the conterminous United States–representing a decade of land cover change information. *Photogramm. Eng. Remote Sens.* **81**, 345–354 (2015).

Acknowledgments

Funding: This work was supported by the National Natural Science Foundation of China (U24A20577; 42401015) (Z.B. and C.H.), Jiangsu Provincial Department of Science and Technology (BK20240599) (Z.B.), National Key Research and Development Program of China (2025YFE0108800) (Z.B.), National Science Foundation (1903722; 1922687) (H.T. and S.P.), and The Engineer Research and Development Center of US Army Corps of Engineers (W912HZ-25-2-0020) (H.T. and X.T.W.). Financial support to Z.B. for this study was in part provided by the U.S. Forest Service Research Participation Program administered by the Oak Ridge Institute for Science and Education through an interagency agreement between the U.S. Department of Energy and the USDA Forest Service. ORISE is managed by Oak Ridge Associated Universities (ORAU). All opinions expressed in this paper are the authors' and do not necessarily reflect the policies and views of USDA, DOE, or ORAU/ORISE. The use of firm, trade, and brand names in this paper is for identification purposes only and does not constitute endorsement. **Author contributions:** Conceptualization: H.T., Z.B., and X.T.W. Methodology: Z.B., S.P., and H.T. Investigation: Z.B. and H.T. Visualization: Z.B. Resources: H.T., G.S., S.P., and Z.B. Funding acquisition: H.T., G.S., S.P., and Z.B. Data curation: Z.B. and H.T. Validation: Z.B., H.T., and X.T.W. Supervision: H.T., G.S., and S.P. Formal analysis: Z.B. and H.T. Software: H.T. and Z.B. Project administration: H.T., S.P., and G.S. Writing–original draft: Z.B. and H.T. Writing–review and editing: Z.B., H.T., G.S., S.P., S.G.M., X.T.W., and C.H. **Competing interests:** The authors declare that they have no competing interests. **Data, code, and materials availability:** All data needed to evaluate the conclusions in the paper are present in the paper and/or the Supplementary Materials. The model-simulated annual nutrient yield results are accessible via https://doi.org/10.5281/zenodo.17796289. This study did not generate any new materials.

Submitted 4 July 2025
Accepted 12 February 2026
Published 20 March 2026
10.1126/sciadv.aea3260

Science Advances

Extreme precipitation reshapes nutrient flows and balance in North America's largest river basin

Zihao Bian, Shufen Pan, Ge Sun, Steven G. McNulty, Xingchen Tony Wang, Changchun Huang, and Hanqin Tian

Sci. Adv. **12** (12), eaea3260. DOI: 10.1126/sciadv.aea3260

Science Advances (ISSN 2375-2548) is published by the American Association for the Advancement of Science. 1200 New York Avenue NW, Washington, DC 20005. The title *Science Advances* is a registered trademark of AAAS.